

Article

Concerning the Role of σ -Hole in Non-Covalent Interactions: Insights from the Study of the Complexes of ArBeO with Simple Ligands

Stefano Borocci ^{1,2} , Felice Grandinetti ^{1,2,*}  and Nico Sanna ^{1,3} 

¹ Dipartimento per la Innovazione nei Sistemi Biologici, Agroalimentari e Forestali (DIBAF), Università della Tuscia, L.go dell'Università, s.n.c., 01100 Viterbo, Italy; borocci@unitus.it (S.B.); n.sanna@unitus.it (N.S.)

² Istituto per i Sistemi Biologici del CNR, Via Salaria, Km 29.500, 00015 Monterotondo, Italy

³ Istituto per la Scienza e Tecnologia dei Plasmi del CNR (ISTP), Via Amendola 122/D, 70126 Bari, Italy

* Correspondence: fgrandi@unitus.it; Tel.: +39-07-6135-7126

Abstract: The structure, stability, and bonding character of some exemplary *L*Ar and *L*-ArBeO (*L* = He, Ne, Ar, N₂, CO, F₂, Cl₂, ClF, HF, HCl, NH₃) were investigated by MP2 and coupled-cluster calculations, and by symmetry-adapted perturbation theory. The nature of the stabilizing interactions was also assayed by the method recently proposed by the authors to classify the chemical bonds in noble-gas compounds. The comparative analysis of the *L*Ar and *L*-ArBeO unraveled geometric and bonding effects peculiarly related to the σ -hole at the Ar atom of ArBeO, including the major stabilizing/destabilizing role of the electrostatic interaction ensuing from the negative/positive molecular electrostatic potential of *L* at the contact zone with ArBeO. The role of the inductive and dispersive components was also assayed, making it possible to discern the factors governing the transition from the (mainly) dispersive domain of the *L*Ar, to the σ -hole domain of the *L*-ArBeO. Our conclusions could be valid for various types of non-covalent interactions, especially those involving σ -holes of respectable strength such as those occurring in ArBeO.

Keywords: σ -hole; bonding analysis; noble-gas chemistry; non-covalent complexes; SAPT analysis



Citation: Borocci, S.; Grandinetti, F.; Sanna, N. Concerning the Role of σ -Hole in Non-Covalent Interactions: Insights from the Study of the Complexes of ArBeO with Simple Ligands. *Molecules* **2021**, *26*, 4477. <https://doi.org/10.3390/molecules26154477>

Academic Editors: Jorge M. C. Marques, Frederico Vasconcellos Prudente and Fernando Pirani

Received: 17 June 2021

Accepted: 20 July 2021

Published: 24 July 2021

Publisher's Note: MDPI stays neutral with regard to jurisdictional claims in published maps and institutional affiliations.



Copyright: © 2021 by the authors. Licensee MDPI, Basel, Switzerland. This article is an open access article distributed under the terms and conditions of the Creative Commons Attribution (CC BY) license (<https://creativecommons.org/licenses/by/4.0/>).

1. Introduction

Non-covalent interactions (NCIs) play a major role in natural and synthetic processes [1–3]. Over the years, the traditional interest for the hydrogen bond (HB) [4,5] has been progressively extended to other NCIs, and greatest attention is, in particular, currently paid to σ -hole [6–9] interactions. The tetrel, pnictogen, chalcogen, and halogen bonds [10,11] (the latter actually rivaling in interest [12,13] that of the HB) are just elder sisters of a large family that embraces most groups of the periodic table [14,15].

σ -holes are regions of charge depletion centered on the outer extension of covalent bonds. They are typically associated with maximum points ($V_{S,max}$) of the molecular electrostatic potential (MEP) [16] (customarily taken at or at around the 0.0010 ea_0^{-3} isodensity surface [17]), and the value of the MEP at $V_{S,max}$ is generally (but not always) positive. Thus, σ -holes typically behave as electrophilic centers, able to promote by contact with a ligand a complex blend of electrostatic, polarization (including induction and charge transfer), and dispersion contributions. The detailed assay of these terms, and of their dependence on the type and the strength of the interaction, are, indeed, of major interest in the study of NCIs. In a recent study [18], we sought to acquire insights into σ -hole effects by exploring the changes occurring when pure (or nearly pure) dispersive contacts were converted into σ -hole interactions. The investigated systems were inspired, in particular, by already-established evidence concerning the complexes of the noble-gas atoms (Ng) with beryllium Lewis acids, particularly BeO [19]. It is, thus, well known that

the NgBeO feature remarkably high binding energies, mainly arising from the appreciable polarization of Ng by BeO, and the ensuing appreciable inductive stabilization. We thus surmised that such a major electronic effect could induce a σ -hole on Ng, and explored the MEP of the NgBeO. The calculations actually confirmed a σ -hole already appreciable in ArBeO, and only slightly more pronounced in KrBeO and XeBeO. We thus focused on the simplest L -ArBeO ($L = \text{He, Ne, Ar, HF}$), and compared their bonding situation with that of their “dispersive” cousins, L Ar [18]. To this end, we employed the symmetry-adapted perturbation theory (SAPT) [20,21], and the method that we recently proposed [22–24] to analyze the bonding situation of Ng compounds. Compared with the L Ar, the L -ArBeO were unraveled as structurally more compact, and this mirrored increased values of the SAPT interaction energies (with respect to the $L + \text{Ar}$ and $L + \text{ArBeO}$ dissociation limits). The two most affected binding components were, in particular, the electrostatic and the inductive, their increases seemingly being related to the electrostatic potential of L , and to its polarizability [18]. Further evidence in this regard came from the failed location of a bound FH-ArBeO, that we ascribed [18], likewise to other “counterintuitive” NCI [25,26], to the unfavorable electrostatic contact between the positive H atom of HF and the positive Ar atom of ArBeO. To reinforce the interpretation, we decided to explore other exemplary L Ar and L -ArBeO, including $L = \text{N}_2, \text{CO, F}_2, \text{Cl}_2, \text{ClF, HCl, and NH}_3$. The MEP of these ligands ranges, in fact, between definitely-negative to definitely-positive values, and this should magnify any effect arising from the contact with the σ -hole of ArBeO. The obtained results, discussed in the present article, actually confirmed this expectation, and furnished insights that could be useful in discussing other types of σ -hole complexes.

The paper is organized as follows. Sections 2 and 3 provide, respectively, a brief account of the methods employed to perform the bonding analysis, and the most relevant computational details. Section 4 first presents the investigated L Ar and L -ArBeO, their predicted data, and an estimate of their accuracy. Then follows the SAPT analysis of the L Ar and L -ArBeO, the former being discussed first as reference systems to best highlight the σ -hole effects occurring in the complexes of L -ArBeO. The L Ar and L -ArBeO are then compared in terms of our proposed descriptors of bonding character. The most relevant conclusions are provided in Section 5.

2. Methods of Bonding Analysis

The bonding analysis was first accomplished by SAPT [20,21]. In this approach, the total Hamiltonian of the dimer is partitioned as $H = F + V + W$, where $F = F_A + F_B$ is the sum of the Fock operators for monomers A and B , V is the intermolecular interaction operator, and $W = W_A + W_B$ is the sum of the Møller-Plesset fluctuation operators. The latter are defined as $W_X = H_X - F_X$, where H_X is the total Hamiltonian of monomer X . The E_{int}^{SAPT} is expanded as a perturbative series, and, in particular, we included the following terms:

$$E_{int}^{SAPT} = E_{elst}^{(10)} + E_{exch}^{(10)} + E_{ind,r}^{(20)} + E_{exch-ind,r}^{(20)} + \delta E_{int,r}^{HF} + E_{elst,r}^{(12)} + {}^t E_{ind}^{(22)} + {}^t E_{exch-ind}^{(22)} + E_{disp}^{(20)} + E_{exch-disp}^{(20)} + E_{elst,r}^{(13)} + \epsilon_{exch}^{(1)}(CCSD) + E_{disp}^{(21)} + E_{disp}^{(22)} \quad (1)$$

the first (1/2) and the second (0/1/2/3) number superscript in parentheses indicating the first-/second-order, and the zeroth-/first-/second-/third-order intramonomer electron correlation correction to V and W , respectively. The notations in subscript indicate the classical (Coulombic) electrostatic energy (*elst*), the exchange term that results from the antisymmetrization of the wave-function (*exch*), the induction energy (*ind*) (including the charge transfer), and the dispersion energy (*disp*). The “*r*” indicates that a given component has been computed by including the coupled Hartree-Fock (HF) response for the perturbed system. The $\delta E_{int,r}^{HF}$ term collects the contributions to the supermolecular HF energy beyond the second-order of intermolecular operator, the ${}^t E_{ind}^{(22)}$ is the part of $E_{ind}^{(22)}$ not included in $E_{ind,r}^{(20)}$ and $\epsilon_{exch}^{(1)}(CCSD) = E_{exch}^{(1)}(CCSD) - E_{exch}^{(10)}$ is the part of $\epsilon_{exch}^{(1)}(\infty)$ with intra-monomer excitations at the CCSD level of theory.

The terms of Equation (1) were grouped so to express E_{int}^{SAPT} as the sum of the electrostatic (E_{elst}), inductive (E_{ind}), dispersive (E_{disp}), and exchange (E_{exch}) components:

$$E_{elst} = E_{elst}^{(10)} + E_{elst,r}^{(12)} + E_{elst,r}^{(13)} \quad (2)$$

$$E_{ind} = E_{ind,r}^{(20)} + E_{exch-ind,r}^{(20)} + {}^tE_{ind}^{(22)} + {}^tE_{exch-ind}^{(22)} + \delta E_{int,r}^{HF} \quad (3)$$

$$E_{disp} = E_{disp}^{(20)} + E_{disp}^{(21)} + E_{disp}^{(22)} + E_{exch-disp}^{(20)} \quad (4)$$

$$E_{exch} = E_{exch}^{(10)} + \epsilon_{exch}^{(1)}(CCSD) \quad (5)$$

Our method of bonding analysis [22–24] relies on the examination of the plotted shape of the local electron energy density $H(\mathbf{r})$ [22,27,28], and on the values that this function takes over the volume Ω_s enclosed by the $s(\mathbf{r}) = 0.4$ reduced-density gradient (RDG) isosurface [29,30] associated with the bond-critical point (BCP) located for a given Ng-X ($X =$ binding partner) from the topological analysis of the electron density $\rho(\mathbf{r})$ [31]. Ancillary indices include the size of Ω_s , the total electronic charge enclosed by Ω_s , $N(\Omega_s)$, the average electron density over Ω_s , $\rho_s(\text{ave}) = N(\Omega_s)/\Omega_s$, and the average, maximum, and minimum values of $H(\mathbf{r})$ over Ω_s , $H_s(\text{ave, max, min})$. As discussed previously [22], the $H(\mathbf{r})$ partitions the atomic space in two well-recognizable regions, namely an inner one of negative values, indicated as $H^-(\mathbf{r})$, and an outer one of positive values, indicated as $H^+(\mathbf{r})$. The boundary of these regions falls at a distance R^- that is typical of each atom; at this distance, $H(\mathbf{r} = R^-) = 0$. Interestingly, when two atoms form a chemical bond, their $H^-(\mathbf{r})$ and $H^+(\mathbf{r})$ regions combine in modes that signal the nature of the interaction. Particularly for the Ng-X bonds, it is possible to distinguish three types of interactions, indicated as A, B, or C.

In interactions of type A, the atoms overlap all the contour lines of their $H^+(\mathbf{r})$ regions, and part of the contour lines of their inner $H^-(\mathbf{r})$ regions, the bond appearing as a continuous region of negative values of $H(\mathbf{r})$, plunged in a zone of positive values. The interaction is topologically-signed by a (3, +1) critical point of the $H(\mathbf{r})$ (denoted as the HCP) falling on the bond axis. Exemplary in this regard is the N-N bond of the N_2 moiety of the N_2 -Ar and the linear N_2 -ArBeO shown in Figure 1. The Ar-Be bond of N_2 -ArBeO is, instead, a showcase of interactions of type B. In these contacts, the $H^-(\mathbf{r})$ region of Ng is, again, overlapped with the $H^-(\mathbf{r})$ region of the binding partner, but (i) no HCP exists on the bond axis, and (ii) the Ng-X inter-nuclear region includes a (more or less wide) region of positive $H(\mathbf{r})$. Finally, the N-Ar bonds of N_2 -Ar and N_2 -ArBeO are illustrative examples of interactions of type C. In contacts like these, the Ng and the binding partner overlap only part of their $H^+(\mathbf{r})$ regions, their $H^-(\mathbf{r})$ regions remaining, instead, perfectly closed, and separated by a (more or less wide) region of positive $H(\mathbf{r})$. The bond thus appears as two clearly distinguishable $H^-(\mathbf{r})$ regions, separated by a region of positive values of $H(\mathbf{r})$.

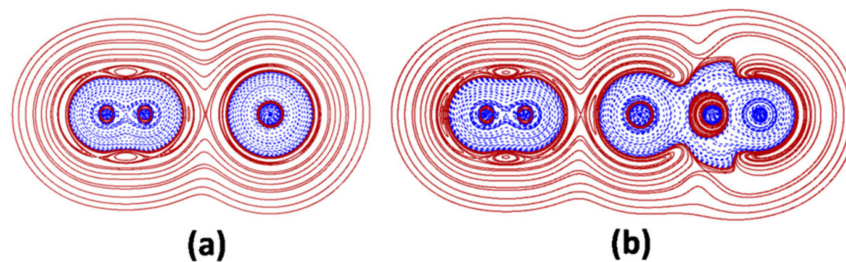


Figure 1. 2D-plots of $H(\mathbf{r})$ in the main plane of (a) N_2 -Ar and (b) linear N_2 -ArBeO (solid/brown and dashed/blue lines correspond, respectively, to positive and negative values).

Any Ng-X is assigned as covalent (Cov) if (i) it is of type A, and (ii) the electron density at the BCP, $\rho(\text{BCP})$ is at least 0.08 ea_0^{-3} . This is the case of the N_2 moiety of the N_2 -Ar and N_2 -ArBeO shown in Figure 1a,b. Any Ng-X not fulfilling these criteria was further assayed

by integrating the $H(r)$ over Ω_s . If the function was, invariably, positive over the entire volume, the interaction was assigned as non-covalent (nCov). If the function was partially or fully negative, the Ng-X was assigned as partially-covalent (pCov), and distinguished as $H^{+/-}$, $H^{-/+}$, and H^- , the superscript indicating that, over Ω_s , the $H(r)$ was ranging from negative to positive, but, on the average, was positive ($H^{+/-}$) or negative ($H^{-/+}$) or, that it is invariably negative (H^-). Interactions of type C involving a single Ng atom, such as the N_2 -Ar shown in Figure 1a, and all the other presently investigated LAr (*vide infra*) were also assayed in terms of the *degree of polarization* of Ng, DoP(Ng). This index measures, in essence, the deformation of the $H^-(r)$ region of Ng arising from the interaction with X [23,32]. The DoP is, in particular, defined by the equation:

$$\text{DoP(Ng)} = \frac{[R_{\text{Ng}}^-(\text{Ng} - \text{X}) - R_{\text{Ng}}^-] \times 100}{R_{\text{Ng}}^-} \quad (6)$$

where $R_{\text{Ng}}^-(\text{Ng} - \text{X})$ is the radius of the $H^-(r)$ region of Ng along the axis formed by Ng and the Ng-X BCP, and R_{Ng}^- is the radius of the $H^-(r)$ region of the free atom. The positive/negative sign of the DoP signal Ng atoms polarized toward/opposite to X, and the magnitude of the DoP is related to the extent of the polarization. Illustrative examples of the effective use of this index are provided in Refs. [23,32].

3. Computational Details

The employed levels of theory were the Møller-Plesset truncated at the second order (MP2) [33], the coupled cluster with inclusion of single and double substitutions, CCSD, and an estimate of connected triples, CCSD(T) [34]. The calculations were performed with the Dunning's correlation consistent aug-cc-pVTZ [35] (denoted here as aVTZ) by explicitly correlating the outer valence electrons (frozen-core approximation). The MP2 and CCSD(T) calculations were performed, respectively, with the Gaussian 09 (G09) (Revision D1) [36], and the CFOUR (version 2.1) [37].

The SAPT [20,21] calculations were performed with the SAPT2016 [38], using the G09 for the integrals calculation. The employed basis set, denoted here as aVTZ/mbf, combined the aVTZ with a set of extra $3s3p2d1f$ mid-bond functions [39,40] (three s and three p functions with exponents 0.9, 0.3, 0.1, two d functions with exponents 0.6 and 0.2, and one f function with exponent 0.3) placed at the mid-point of any Ar-X distance (X = atom closest to Ar in the linear complexes, or center-of-mass of X_2 in the T-shaped complexes).

The functions investigated in the bonding analysis were the $\rho(r)$ [31], the $H(r)$ [22,27,28], and the RDG and its related NCI indices [29,30]. The $\rho(r)$ is defined by the equation [31]:

$$\rho(r) = \sum_i \eta_i |\varphi_i(r)|^2 \quad (7)$$

where η_i is the occupation number of the natural orbital φ_i , in turn expanded as a linear combination of the basis functions.

The $H(r)$ is the sum of the kinetic energy density $G(r)$ and the potential energy density $V(r)$:

$$H(r) = G(r) + V(r) \quad (8)$$

The presently employed definition [31,41] of the $G(r)$ is given by the equation:

$$G(r) = \frac{1}{2} \sum_{i=1} \eta_i |\nabla \varphi_i(r)|^2 \quad (9)$$

where the sum runs over all the occupied natural orbitals φ_i of occupation numbers η_i . The potential energy density $V(r)$ is evaluated [31] from the local form of the virial theorem:

$$V(r) = \frac{1}{4} \nabla^2 \rho(r) - 2G(r) \quad (10)$$

The RDG is defined by the equation [29,30]:

$$s(\mathbf{r}) = \frac{|\nabla\rho(\mathbf{r})|}{2(3\pi^2)^{\frac{1}{3}} \times \rho(\mathbf{r})^{\frac{4}{3}}} \quad (11)$$

Low-value $s(\mathbf{r})$ isosurfaces (typically 0.3–0.6) appear among atoms undergoing any type of interaction, the NCIs emerging, in particular, by considering the spatial regions of low $\rho(\mathbf{r})$. The low- $s(\mathbf{r})$ /low- $\rho(\mathbf{r})$ isosurfaces are, in turn, mapped in terms of the sign (λ_2) \times $\rho(\mathbf{r})$, λ_2 being the second eigenvalue ($\lambda_1 < \lambda_2 < \lambda_3$) of the Hessian matrix of $\rho(\mathbf{r})$. In essence, the sign of λ_2 is used to distinguish between attractive ($\lambda_2 < 0$) and repulsive ($\lambda_2 > 0$) interactions, and the value of $\rho(\mathbf{r})$ is exploited to rank the corresponding strength. In the present study, we also calculated the integral of a given property P (particularly the $\rho(\mathbf{r})$ and the $H(\mathbf{r})$) over the volume Ω_s enclosed by the $s(\mathbf{r}) = 0.4$ isosurface at around the BCP located on any Ar-X bond path, $P(\Omega_s)$. This integration was accomplished by producing an orthogonal grid of points that enclosed the isosurface and applying the formula:

$$P(\Omega_s) = \sum_{i(\text{RDG} < s)} P(\mathbf{r}_i) d_x d_y d_z \quad (12)$$

where $P(\mathbf{r}_i)$ is the value of P at the grid point \mathbf{r}_i , and d_x , d_y , and d_z are the grid step sizes in the x , y , and z directions, respectively ($d_x = d_y = d_z = 0.025 a_0$). The summation is carried out on all grid points \mathbf{r}_i having $\text{RDG} < s$.

The $\rho(\mathbf{r})$, the $H(\mathbf{r})$, and the $s(\mathbf{r})$ were analyzed with the Multiwfn (version 3.8.dev) [42] using the MP2/aVTZ wave functions stored in the wfx files generated with the G09 or the CCSD(T)/aVTZ wave functions stored in the molden files generated with CFOUR, and subsequently formatted with the Molden2AIM utility [43]. The two-(2D) plots of the $H(\mathbf{r})$ were also produced with the Multiwfn, and included the standard contour lines belonging to the patterns $\pm k \times 10^n$ ($k = 1, 2, 4, 8; n = -5 \div 6$), together with the contour lines corresponding to the critical points specifically located from the topological analysis of the $H(\mathbf{r})$.

4. Results and Discussion

4.1. The Investigated LAr and L-ArBeO: Predicted Data and Their Accuracy

The investigated LAr included the diatomic HeAr, NeAr, and ArAr, the linear and T-shaped (N₂)Ar, (F₂)Ar, and (Cl₂)Ar, the linear isomeric (CO)Ar, (FCl)Ar, (HF)Ar, and (HCl)Ar, and the H₃N-Ar structure of C_{3v} symmetry. These species were explored at both the MP2/aVTZ and CCSD(T)/aVTZ level of theory, and invariably characterized as true minima on the potential energy surface (PES). The only exceptions were the OC-Ar and the H₃N-Ar, both featuring a doubly degenerate imaginary absorption (number of imaginary frequencies NIMAG = 2). As shown in Table S1 of the Supplementary Materials, the MP2/aVTZ and CCSD(T)/aVTZ harmonic frequencies of the LAr were, invariably, quite similar, and the MP2/aVTZ Ar-X distances featured a mean unsigned deviation (MUD) from the CCSD(T)/aVTZ values of only 0.0385 Å. We also ascertained (see Table S1 of Supplementary Materials) the high similarity between the MP2/aVTZ and CCSD(T)/aVTZ predicted data of the simplest He-ArBeO, Ne-ArBeO, Ar-ArBeO, and HF-ArBeO. Based on these findings, all the other L-ArBeO ($L = \text{N}_2, \text{CO}, \text{F}_2, \text{Cl}_2, \text{ClF}, \text{HCl}, \text{NH}_3$) were investigated at the predictably accurate MP2/aVTZ. The connectivities and bond distances of all the presently investigated LAr and L-ArBeO are thus shown in Figure 2 (their Cartesian coordinates are also available as Data S1 of the Supplementary Materials). Their CCSD/aVTZ T_1 diagnostics (the norm of the vector \mathbf{t}_1 of the single-excitation amplitudes from the CCSD calculation divided by the square root of the number of correlated electrons N , $T_1 = \sqrt{\frac{t_1^2}{N}}$) resulted invariably within the accepted threshold of 0.02 [44], thus confirming the validity of a mono-determinantal description of their wave functions.

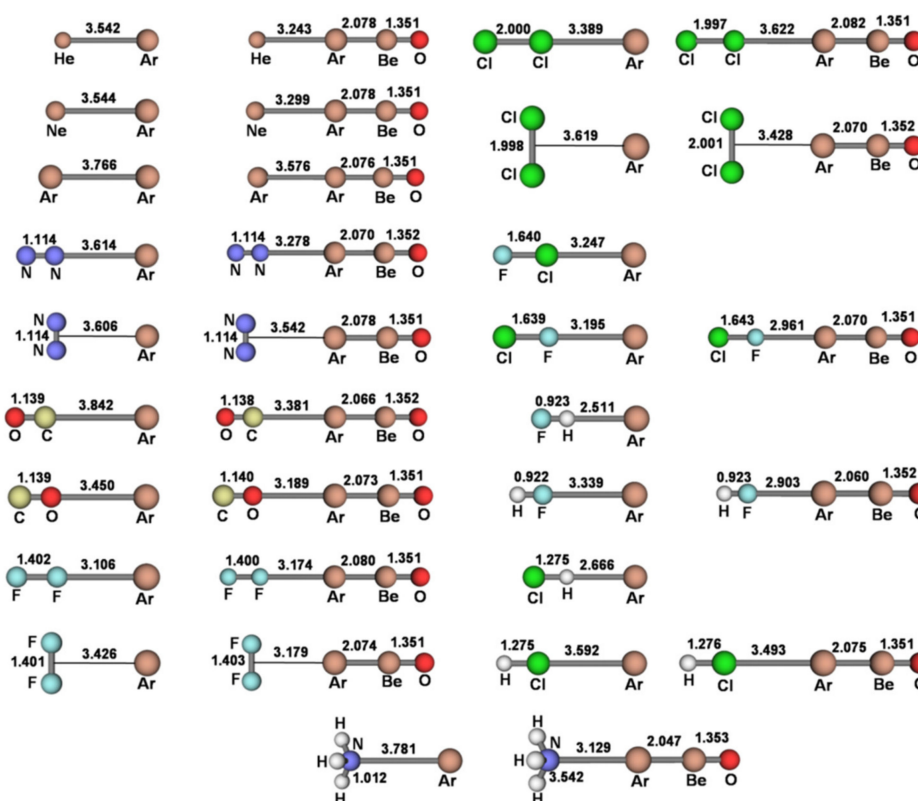


Figure 2. MP2/aVTZ connectivities and bond distances (Å) of the L Ar and L -ArBeO ($L = \text{He, Ne, Ar, N}_2, \text{CO, F}_2, \text{Cl}_2, \text{ClF, HF, HCl, NH}_3$).

The MP2/aVTZ structures of the L Ar and L -ArBeO were then employed to perform the SAPT calculations (dissociation limits: $L + \text{Ar}$ and $L + \text{ArBeO}$), and the bonding analysis. The obtained results are shown in Tables 1 and 2. For the L Ar, the computed E_{int}^{SAPT} were, in general, well consistent ($\text{MUD} = 0.02 \text{ kcal mol}^{-1}$) with other accurate theoretical estimates already available from the literature [45–55]. In addition, as shown in Table S2 of the Supplementary Materials, the results of the bonding analysis of the L Ar performed at the MP2/aVTZ and CCSD(T)/aVTZ levels of theory furnished strictly similar results. These findings, overall, support the good accuracy of the data reported in Tables 1 and 2. Their detailed discussion is provided in the forthcoming paragraphs.

Table 1. SAPT analysis (kcal mol^{-1}) of the L Ar (dissociation limits: $L + \text{Ar}$) and L -ArBeO (dissociation limits: $L + \text{ArBeO}$) (see Figure 2) performed with the aVTZ/mbf basis set. $E_{elst}(\%)$, $E_{ind}(\%)$, and $E_{disp}(\%)$ are the percentage contributions, respectively, of $|E_{elst}|$, $|E_{ind}|$, and $|E_{disp}|$ to $(|E_{elst}| + |E_{ind}| + |E_{disp}|)$.

	E_{elst}	E_{ind}	E_{disp}	E_{exch}	E_{int}^{SAPT} a	Lit.	$E_{elst}(\%)$	$E_{ind}(\%)$	$E_{disp}(\%)$	DoP(Ar) b
HeAr	−0.0119	−0.0040	−0.1049	0.0638	−0.0570	−0.0588 c	9.85	3.35	86.80	0.026
He-ArBeO	−0.0204	−0.0432	−0.1686	0.1218	−0.1104		8.80	18.61	72.59	
NeAr	−0.0433	−0.0037	−0.2306	0.1534	−0.1242	−0.1342 d	15.61	1.34	83.05	0.039
Ne-ArBeO	−0.0507	−0.0797	−0.3371	0.2561	−0.2114		10.85	17.04	72.11	
ArAr	−0.1332	−0.0179	−0.5641	0.4311	−0.2841	−0.2846 e	18.62	2.50	78.88	0.099
Ar-ArBeO	−0.1745	−0.2428	−0.7345	0.6422	−0.5096		15.15	21.08	63.77	
N ₂ -Ar	−0.1074	−0.0189	−0.5284	0.4039	−0.2508	−0.2221 f	16.41	2.88	80.71	−0.14
N ₂ -ArBeO	−0.9782	−0.3132	−0.9032	1.0386	−1.1560		44.57	14.27	41.16	
N ₂ -Ar (T ^g)	−0.1635	−0.0223	−0.6912	0.5682	−0.3088	−0.2913 f	18.64	2.54	78.82	0.36
N ₂ -ArBeO (T)	0.2296	−0.1944	−0.7061	0.5104	−0.1605		20.32	17.20	62.48	
OC-Ar	−0.1063	−0.0191	−0.4698	0.3506	−0.2446	−0.2078 h	17.86	3.21	78.93	−0.29
OC-ArBeO	−1.5489	−0.3531	−0.9869	1.3982	−1.4907		53.61	12.22	34.16	
CO-Ar	−0.1224	−0.0290	−0.5916	0.4618	−0.2812	−0.2391 h	16.47	3.91	79.62	−0.034
CO-ArBeO	−0.9018	−0.3204	−0.8840	0.8791	−1.2271		42.81	15.21	41.97	
F ₂ -Ar	−0.2343	−0.1155	−0.8264	0.8015	−0.3747	−0.3510 i	19.92	9.82	70.26	0.69
F ₂ -ArBeO	0.4667	−0.2444	−0.6561	0.3806	−0.0532		34.14	17.86	48.00	
F ₂ -Ar (T)	−0.1406	−0.0133	−0.6521	0.4774	−0.3286	−0.3146 i	17.44	1.65	80.91	0.013

Table 1. Cont.

	E_{elst}	E_{ind}	E_{disp}	E_{exch}	E_{int}^{SAPT} ^a	Lit.	$E_{elst}(\%)$	$E_{ind}(\%)$	$E_{disp}(\%)$	DoP(Ar) ^b
F₂-ArBeO (T)	−0.3956	−0.2249	−0.9411	0.8385	−0.7231		25.33	14.40	60.27	
Cl ₂ -Ar	−0.4113	−0.2373	−1.3498	1.3329	−0.6655	−0.6487 ^j	20.58	11.87	67.54	1.28
Cl₂-ArBeO	1.0857	−0.3846	−0.8325	0.3932	0.2618		47.15	16.70	36.15	
Cl ₂ -Ar (T)	−0.3778	−0.0603	−1.3592	1.1461	−0.6512	−0.6314 ^j	21.02	3.35	75.63	0.20
Cl₂-ArBeO (T)	−0.9942	−0.6121	−1.7521	1.7508	−1.6076		29.60	18.22	52.17	
FCl-Ar	−0.5476	−0.5337	−1.6006	1.8462	−0.8357	−0.8101 ^k	20.42	19.90	59.68	1.89
ClF-Ar	−0.2064	−0.0716	−0.8296	0.6875	−0.4201	−0.3687 ^k	18.63	6.47	74.90	0.021
ClF-ArBeO	−1.2759	−0.4951	−1.1938	1.2087	−1.7561		43.04	16.70	40.27	
FH-Ar	−0.2437	−0.8019	−0.9663	1.4098	−0.6020	−0.6037 ^l	12.11	39.86	48.03	3.80
HF-Ar	−0.1203	−0.0705	−0.5234	0.4182	−0.2960	−0.3067 ^l	16.84	9.87	73.29	−0.54
HF-ArBeO	−3.5413	−0.4587	−1.1374	1.6639	−3.4735		68.93	8.92	22.14	
ClH-Ar	−0.3268	−0.4413	−1.0998	1.3561	−0.5118	−0.5050 ^m	17.50	23.63	58.87	2.45
HCl-Ar	−0.2153	−0.0611	−0.8788	0.7188	−0.4364	−0.4288 ^m	18.64	5.29	76.07	0.52
HCl-ArBeO	−0.3947	−0.3613	−0.9692	0.7563	−0.9689		22.88	20.94	56.18	
H ₃ N-Ar	−0.2052	−0.1364	−0.5726	0.5809	−0.3333	−0.2966 ⁿ	22.45	14.92	62.63	−0.98
H₃N-ArBeO	−6.8566	−1.0230	−1.6735	4.1151	−5.4380		71.77	10.71	17.52	

^a $E_{int}^{SAPT} = E_{elst} + E_{ind} + E_{disp} + E_{exch}$; ^b defined by Equation (4); ^c Ref. [45]; ^d Ref. [46]; ^e Ref. [47]; ^f Ref. [48]; ^g T-shaped; ^h Ref. [49]; ⁱ Ref. [50]; ^j Ref. [51]; ^k Ref. [52]; ^l Ref. [53]; ^m Ref. [54]; ⁿ Ref. [55].

Table 2. MP2/aVTZ properties of the nCov(C) bonds (see text) of the LAr and L-ArBeO (see Figure 2). $N(\Omega_s)$, $\rho_s(\text{ave})$, and $H_s(\text{ave}/\text{max}/\text{min})$ are, respectively, the total electronic charge (me), the average electron density ($e a_0^{-3}$), and the average, maximum, and minimum of $H(r)$ (hartree a_0^{-3}) over the volume Ω_s (a_0^3) enclosed by the $s(r) = 0.4$ isosurface around the BCP.

Bond		Ω_s	$N(\Omega_s)$	$\rho_s(\text{ave})$	$H_s(\text{ave}/\text{max}/\text{min})$
He-Ar	HeAr	0.0212	0.024	0.0011	0.00040/0.00042/0.00038
	He-ArBeO	0.0234	0.043	0.0018	0.00079/0.00082/0.00076
Ne-Ar	NeAr	0.0316	0.063	0.0020	0.00059/0.00061/0.00057
	Ne-ArBeO	0.0372	0.11	0.0030	0.00084/0.00103/0.00090
Ar-Ar	ArAr	0.0948	0.27	0.0029	0.00074/0.00078/0.00069
	Ar-ArBeO	0.0942	0.35	0.0038	0.00113/0.00122/0.00105
N-Ar	N ₂ -Ar	0.0788	0.22	0.0028	0.00076/0.00080/0.00071
	N ₂ -ArBeO	0.0904	0.46	0.0051	0.00162/0.00172/0.00150
	N ₂ -Ar (T ^a)	0.1570	0.46	0.0029	0.00075/0.00082/0.00067
	N ₂ -ArBeO (T)	0.1344	0.40	0.0030	0.00086/0.00093/0.00078
C-Ar	OC-Ar	0.0914	0.21	0.0023	0.00060/0.00063/0.00056
	OC-ArBeO	0.1203	0.64	0.0053	0.00150/0.00167/0.00139
O-Ar	CO-Ar	0.0736	0.24	0.0032	0.00086/0.00091/0.00080
	CO-ArBeO	0.0785	0.40	0.0051	0.00159/0.00168/0.00148
F-Ar	F ₂ -Ar	0.0966	0.46	0.0047	0.00154/0.00176/0.00137
	F ₂ -ArBeO	0.0686	0.24	0.0035	0.00124/0.00134/0.00113
	F ₂ -Ar (T)	0.2052	0.59	0.0029	0.00068/0.00076/0.00058
	F ₂ -ArBeO (T)	0.2254	0.95	0.0042	0.00111/0.00126/0.00096
Cl-Ar	Cl ₂ -Ar	0.1687	0.90	0.0053	0.00153/0.00165/0.00139
	Cl ₂ -ArBeO	0.1139	0.32	0.0028	0.00095/0.00101/0.00087
	Cl ₂ -Ar (T)	0.4444	1.56	0.0035	0.00088/0.00095/0.00076
	Cl ₂ -ArBeO (T)	0.4482	2.08	0.0046	0.00127/0.00142/0.00111
Cl-Ar	FCl-Ar	0.2167	1.44	0.0067	0.00184/0.00199/0.00165
F-Ar	ClF-Ar	0.0866	0.38	0.0043	0.00121/0.00132/0.00111
	ClF-ArBeO	0.0920	0.61	0.0066	0.00212/0.00233/0.00193
H-Ar	FH-Ar	0.0777	0.65	0.0084	0.00148/0.00158/0.00134
F-Ar	HF-Ar	0.0700	0.23	0.0032	0.00092/0.00097/0.00086
	HF-ArBeO	0.0936	0.73	0.0078	0.00259/0.00286/0.00234
H-Ar	ClH-Ar	0.0922	0.64	0.0069	0.00129/0.00140/0.00123
Cl-Ar	HCl-Ar	0.1268	0.46	0.0037	0.00112/0.00120/0.00102
	HCl-ArBeO	0.1170	0.47	0.0041	0.00135/0.00145/0.00124
N-Ar	H ₃ N-Ar	0.1113	0.31	0.0028	0.00055/0.00063/0.00051
	H ₃ N-ArBeO	0.1815	1.65	0.0091	0.00185/0.00209/0.00168

^a T-shaped.

4.2. SAPT Analysis of the LAr: The Role of the MEP of L

We first discuss the SAPT data of the LAr (dissociation limit: $L + \text{Ar}$). The complexes of Ng with neutral species are, in general, perceived as typical van der Waals molecules [56], held together by the favorable balance between dispersion and exchange repulsion. The leading interaction components of any LNg may include, however, electrostatic, inductive, and even charge-transfer contributions [57]. Illustrative in this regard are also the presently-investigated LAr, whose decomposed E_{int}^{SAPT} (see Table 1) clearly unraveled an invariably major E_{disp} , but also non-negligible contributions of E_{elst} and E_{ind} . Especially relevant in the present context is the dependence of these terms on the MEP of L, particularly on the values that this function takes for the various ligands at the $V_{S,max}$ or $V_{S,min}$ occurring on the outer elongation of the bond axis or perpendicular to it. We could locate these critical points on any probed isodensity surface (namely 0.0005, 0.0010, 0.0015, and 0.0020 ea_0^{-3}), and, as shown in Table S3 of the Supplementary Materials, the values of the MEP at these points were only less sensitive to the employed geometry (experimental, MP2/aVTZ or CCSD(T)/aVTZ), and to the method used to calculate the electron density (MP2/aVTZ or CCSD(T)/aVTZ). The forthcoming discussion is based, in particular, on the values quoted in Table 3, computed at the MP2/aVTZ 0.0010 ea_0^{-3} isodensity surfaces using the MP2/aVTZ-optimized geometries.

Table 3. MP2/aVTZ values (kcal mol^{-1} , 0.0010 ea_0^{-3} isodensity surface) at the minimum ($V_{S,Min}$) or maximum ($V_{S,Max}$) points of the MEP calculated at the MP2/aVTZ optimized geometries (\AA and $^\circ$), and experimental polarizabilities α (\AA^3) of L.

L	MEP Point		R/ θ	$\bar{\alpha}$	$\alpha_{ }^a$	α_{\perp}^b
N₂	$V_{S,Min}(\text{N}): -8.53$	$V_{S,Max}(\text{perp}): 7.82$	1.114	1.75 ^c	2.20 ^d	1.52 ^d
CO	$V_{S,Min}(\text{C}): -14.04$	$V_{S,Min}(\text{O}): -4.12$	1.139	1.95 ^e	2.31 ^e	1.77 ^e
F₂	$V_{S,Max}(\text{F}): 16.57$	$V_{S,Max}(\text{perp}): 0.76$	1.401	1.25 ^f	1.84 ^f	0.96 ^f
Cl₂	$V_{S,Max}(\text{Cl}): 25.50$	$V_{S,Max}(\text{perp}): 1.26$	1.999	4.59 ^g	6.27 ^g	3.75 ^g
ClF	$V_{S,Max}(\text{Cl}): 40.94$	$V_{S,Max}(\text{F}): -1.86$	1.639	2.68 ^h	3.37 ⁱ	2.34 ^j
HF	$V_{S,Max}(\text{H}): 68.78$	$V_{S,Max}(\text{F}): -18.91$	0.922	0.83 ^k	0.94 ^k	0.77 ^k
HCl	$V_{S,Max}(\text{H}): 45.38$	$V_{S,Max}(\text{Cl}): 9.00$	1.275	2.58 ^l	2.74 ^l	2.50 ^l
NH₃	$V_{S,Min}(\text{N}): -37.25$		1.012/106.8	2.15 ^m		

^a Component along the bond axis; ^b component perpendicular to the bond axis; ^c calculated as $\bar{\alpha} = \frac{(\alpha_{||} + 2\alpha_{\perp})}{3}$; ^d Ref. [58]; ^e Ref. [59]; ^f Ref. [60]; ^g Ref. [61]; ^h evaluated by the empirical method proposed in Ref. [62]; ⁱ Ref. [63]; ^j calculated as $\alpha_{\perp} = \frac{(3\bar{\alpha} - \alpha_{||})}{2}$; ^k Ref. [64]; ^l Ref. [65]; ^m Ref. [66].

We first note from Figure 2 the strict relationship between the connectivity of any LAr and the position of the $V_{S,max}$ or $V_{S,min}$ of the involved ligand. In essence, the anisotropy of the electron density of L directed the Ar atom toward the stationary point(s) on the PES. Depending on L, however, the potential locally-experienced by Ar was quite different, and ranged (see Table 3) from the definitely negative one at the $V_{S,min}(\text{N})$ of NH_3 ($-37.25 \text{ kcal mol}^{-1}$) to the definitely positive one at the $V_{S,max}(\text{H})$ of HF ($68.78 \text{ kcal mol}^{-1}$), passing through the only slightly-positive values of He ($1.26 \text{ kcal mol}^{-1}$), Ne ($1.02 \text{ kcal mol}^{-1}$), Ar ($1.85 \text{ kcal mol}^{-1}$), and at the $V_{S,max}(\text{perp})$ of F_2 ($0.76 \text{ kcal mol}^{-1}$) and Cl_2 ($1.26 \text{ kcal mol}^{-1}$). Interestingly, as expected from the results of our recent studies on other numerous Ng complexes [23,32], these different local fields produced a well-recognizable effect, namely the polarization of Ar in modes and extents that strictly mirror the values of the MEP. This phenomenon is effectively caught by the DoP(Ar) (*vide supra*) of the various LAr (see Table 1) that is positively correlated with the MEP at the $V_{S,max}$ or $V_{S,min}$ of L (see Table 3). This is graphically shown in Figure 3.

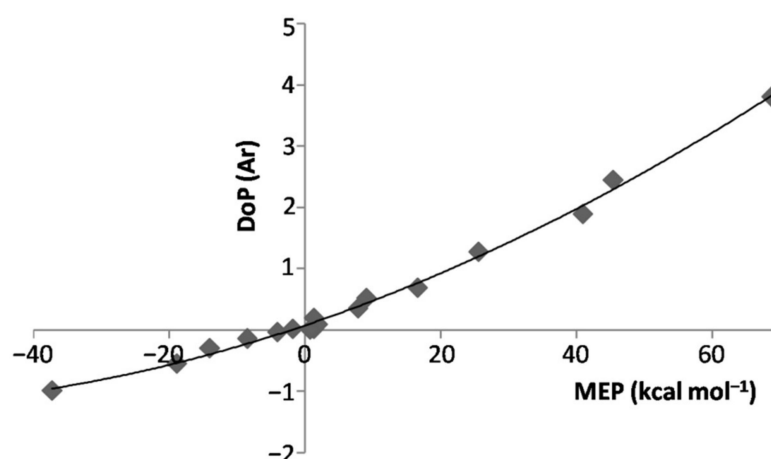


Figure 3. DoP(Ar) of the LAr vs. MEP at the $V_{S,max}/V_{S,min}$ of L.

In essence, when exposed to the MEP of the ligand, the Ar atom polarized toward/opposite to it, the effect increasing by increasing the magnitude of the experienced positive/negative MEP. However, the polarization of Ar was, expectedly, the major physical phenomenon behind the inductive component of the interaction. As a matter of fact, as shown in Figure S1 of the Supplementary Materials, for both positive and negative values of the MEP of L, the E_{ind} of the various LAr generally increased by increasing the magnitude of the MEP. This positive correlation becomes even more clear by inspecting Figure 4, showing the dependence on the MEP of L of the percentage contribution of E_{ind} to the total attractive part of the SAPT interaction, $E_{ind}(\%)$. On the other hand, neither the absolute E_{elst} nor the percentage contribution $E_{elst}(\%)$ of the LAr correlated with the MEP of L. This was, indeed, not unexpected, as this term solely arises from non-specific electrostatic interactions between the frozen densities of L and of the apolar Ar. One also notes from Table 1 that the $E_{elst}(\%)$ of the various LAr spanned in the small range between ca. 12 and ca. 22%. These nearly constant contributions produced an inverse dependence between $E_{ind}(\%)$ and $E_{disp}(\%)$ (Figure S2 of Supplementary Materials), a positive correlation between $E_{disp}(\%)$ and the MEP of L (Figure S3 of Supplementary Materials), and the positive correlation shown in Figure 5 between the E_{ind}/E_{disp} ratio of the LAr, and the MEP of L. The absolute values of E_{disp} are, in any case, totally uncorrelated with the MEP. The dispersion is, in fact, also a form of polarization [67], but different in origin from the inductive effects exerted by the MEP.

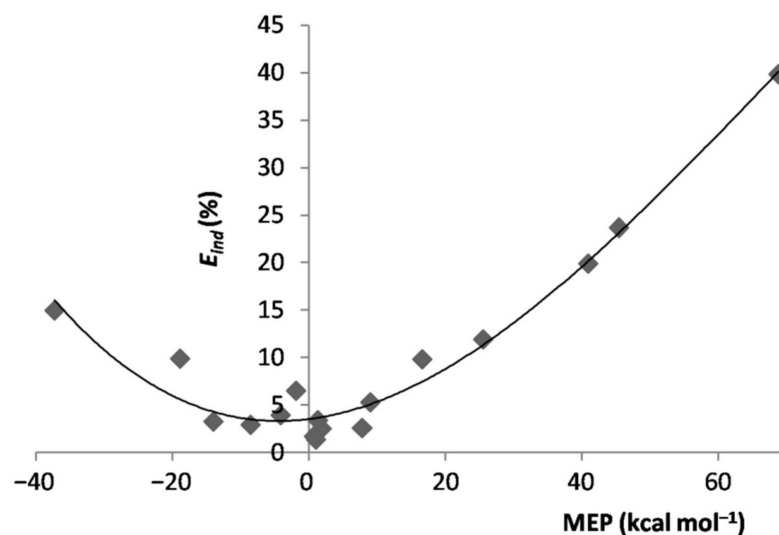


Figure 4. $E_{ind}(\%)$ of the LAr vs. MEP at the $V_{S,max}/V_{S,min}$ of L.

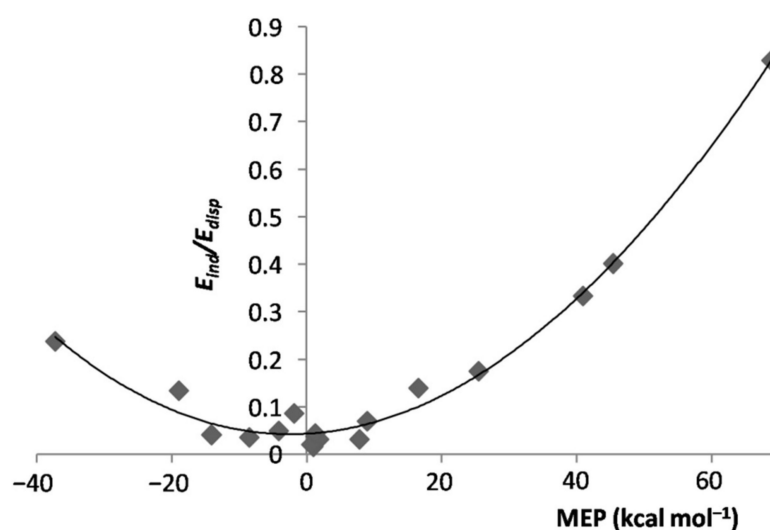


Figure 5. E_{ind}/E_{disp} ratio of the LArvs. MEP at the $V_{S,max}/V_{S,min}$ of L.

The ligation of BeO to the Ar atom of any LAr produced major structural and stability effects that were clearly referable to the σ -hole occurring at Ar. This is best discussed in the subsequent paragraph.

4.3. From the LAr to the L-ArBeO: The Role of the σ -Hole of ArBeO

The only slightly positive electrostatic potential of Ar (1.85 kcal mol⁻¹ at the MP2/aVTZ0.0010 ea_0^{-3} isodensity surface) was dramatically affected by the ligation with BeO. As shown in Figure 6a, plotting the MEP of ArBeO in the scale between -20 and 48 kcal mol⁻¹, the Ar atom appeared as definitely positive, with a seemingly uniform MEP at around 48 kcal mol⁻¹. However, as shown in Figure 6b, using a narrower scale between 42.0 and 50.0 kcal mol⁻¹, the MEP of Ar emerged as clearly anisotropic, and featured a $V_{S,max}$ of 50.9 kcal mol⁻¹ on the outer prolongation of the Ar-Be axis. This maximum signs a σ -hole arising from the polarization of Ar by BeO toward the inner region of the Ar-Be bond.

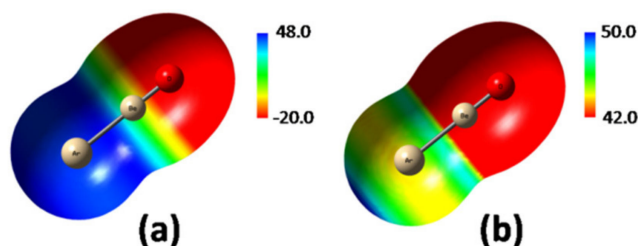


Figure 6. MP2/aVTZ MEP (0.0010 ea_0^{-3} isodensity surface) of ArBeO plotted using a wider (a) and narrower (b) scale (values in kcal mol⁻¹).

The major ensuing effects are best appreciated by comparing the SAPT data of the L-ArBeO (dissociation limit: $L + \text{ArBeO}$) with those of the corresponding LAr. We first discuss the changes occurring in the electrostatic component of the interaction. In this regard, based on the data quoted in Table 1, it is possible to recognize three major situations. Thus, when Ar is in contact with ligands whose MEP at the $V_{S,max}$ or $V_{S,min}$ was negative or only slightly-positive (up to less than 2 kcal mol⁻¹), the E_{elst} of the L-ArBeO was invariably negative, and higher in magnitude than that of the corresponding LAr. The E_{int}^{SAPT} was also definitely more negative than that of the LAr, and the Ar-X distance was shorter by ca. 0.2–0.4 Å, the contraction arriving up to ca. 0.65 Å for $L = \text{NH}_3$. These systems include the Ng-ArBeO (Ng = He, Ne, Ar), the linear N₂-ArBeO, OC-ArBeO, CO-ArBeO, ClF-ArBeO, and HF-ArBeO, the T-shaped F₂-ArBeO and Cl₂-ArBeO, and the C_{3v} isomer H₃N-ArBeO. All these species are also characterized as true minima on the MP2/aVTZ PES,

the only exception being the T-shaped $\text{Cl}_2\text{-ArBeO}$, featuring a single imaginary frequency ($\text{NIMAG} = 1$) (see Table S1 of the Supplementary Materials). According to the electrostatic model of NCIs [67,68], these contacts must be viewed as “intuitive” interactions [25,26] driven from the favorable attraction between MEPs of opposite sign. When Ar was in contact with $V_{S,\text{max}}$ or $V_{S,\text{min}}$ featuring positive values of the MEP up to ca. 25 kcal mol^{-1} , the E_{elst} of the $L\text{-ArBeO}$ was lower in magnitude than that of the corresponding $L\text{Ar}$, and even positive. The $E_{\text{int}}^{\text{SAPT}}$ was also less negative than that of the $L\text{Ar}$, or even positive. These systems include the T-shaped $\text{N}_2\text{-ArBeO}$, and the linear $\text{F}_2\text{-ArBeO}$ and $\text{Cl}_2\text{-ArBeO}$, invariably characterized as higher-order saddle points on the corresponding PES (see Table S1 of the Supplementary Materials). All these features are typical of “counterintuitive” complexes [25,26], whose bound characters arise from inductive and dispersive components still sufficient to compensate for the repulsive electrostatic contribution from MEPs of the same sign. Finally, the contact of Ar with ligands featuring definitely positive values of the MEP at their $V_{S,\text{max}}$ was totally repulsive, and the corresponding $L\text{-ArBeO}$ were unbound on the PES. This happened, in particular, for the FH-ArBeO , FCl-ArBeO , and ClH-ArBeO . The major role of the MEP of L in determining these different situations clearly emerges by examining Figure 7, showing the positive correlation between this quantity and the E_{elst} of the $L\text{-ArBeO}$. The percentage contributions $E_{\text{elst}}(\%)$, covering the wide range between ca. 9 and ca. 72%, were also regularly dependent on the MEP of L (see Figure S4 of the Supplementary Materials).

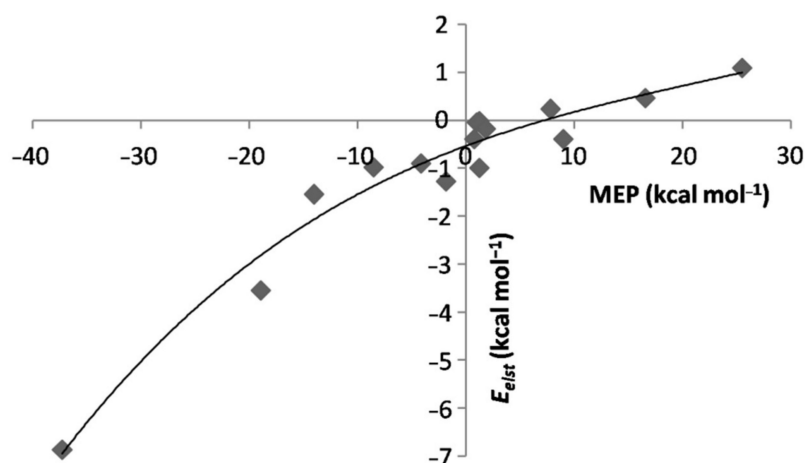


Figure 7. E_{elst} of the $L\text{-ArBeO}$ vs. MEP at the $V_{S,\text{max}}/V_{S,\text{min}}$ of L .

The major role of the electrostatic component in determining the stability of the $L\text{-ArBeO}$ clearly emerges by examining some exemplary situations. Thus, the highly negative $V_{S,\text{Min}}(\text{N})$ of NH_3 of $-37.25 \text{ kcal mol}^{-1}$ produced a E_{elst} of the $\text{H}_3\text{N-ArBeO}$ as negative as ca. $-6.9 \text{ kcal mol}^{-1}$ (see Table 1). The E_{elst} of the $\text{H}_3\text{N-Ar}$ was, instead, only ca. $-0.2 \text{ kcal mol}^{-1}$, and the difference of $-6.7 \text{ kcal mol}^{-1}$ decisively contributed to the huge increase of the $E_{\text{int}}^{\text{SAPT}}$ when going from $\text{H}_3\text{N-Ar}$ ($-0.33 \text{ kcal mol}^{-1}$) to $\text{H}_3\text{N-ArBeO}$ ($-5.4 \text{ kcal mol}^{-1}$). It is also of interest to compare the $\text{N}_2\text{-ArBeO}$ with the isomeric OC-ArBeO and CO-ArBeO . The $V_{S,\text{Min}}(\text{N})$ of N_2 , $-8.53 \text{ kcal mol}^{-1}$ was more negative than the $V_{S,\text{Min}}(\text{O})$ of CO , -4.12 , and this produced a E_{elst} of $\text{N}_2\text{-ArBeO}$ ($-0.98 \text{ kcal mol}^{-1}$) that was more negative than that of the CO-ArBeO ($-0.90 \text{ kcal mol}^{-1}$). This is opposite to the trend across $\text{N}_2\text{-Ar}$ and CO-Ar , whose E_{elst} amounts to ca. -0.11 and $-0.12 \text{ kcal mol}^{-1}$, respectively. Conversely, the $V_{S,\text{Min}}(\text{C})$ of CO of $-14.04 \text{ kcal mol}^{-1}$ produced a E_{elst} of OC-ArBeO (ca. $-1.55 \text{ kcal mol}^{-1}$) that was more negative than that of $\text{N}_2\text{-ArBeO}$, the difference of $-0.57 \text{ kcal mol}^{-1}$ decisively determining the $E_{\text{int}}^{\text{SAPT}}$ of OC-ArBeO as more negative than that of $\text{N}_2\text{-ArBeO}$ (-1.49 vs. $-1.16 \text{ kcal mol}^{-1}$). As a matter of fact, in the absence of this electrostatic stabilization, the $E_{\text{int}}^{\text{SAPT}}$ of $\text{N}_2\text{-Ar}$ and OC-Ar were, essentially, the same (-0.25 and $-0.24 \text{ kcal mol}^{-1}$, respectively).

As for the inductive component of the interaction, its magnitude invariably increased (became more negative) when going from any LAr to the corresponding $L-ArBeO$. At variance with the LAr , however, the values of E_{ind} were not correlated with the MEP of the L . This finding was, indeed, not unexpected, as this energy term expectedly mirrors the mutual polarization of L and $ArBeO$. This suggestion is partially supported by the graph plotted in Figure S5 of the Supplementary Materials, showing the dependence of the E_{ind} of the $L-ArBeO$ on the experimental polarizability α of L [60–68] (see Table 3). For the majority of the complexes, the two quantities were, indeed, positively correlated. There were, however, at least three major deviations ($HF-ArBeO$, $H_3N-ArBeO$, and the linear $Cl_2-ArBeO$), whose occurrences clearly suggest that various factors conceivably contributed to this energy component. In any case, for any $L-ArBeO$, the *percentage* contribution $E_{ind}(\%)$, was only minor, and spanned over the rather limited range of ca. 9–21% (see Table 1). As shown in Figures S6 and S7 of the Supplementary Materials, this produced an inverse relationship between $E_{elst}(\%)$ and $E_{disp}(\%)$, and a positive correlation between the $E_{disp}(\%)$ of the various $L-ArBeO$, and the MEP of L . This also produced the positive correlation shown in Figure 8 between the ratio E_{elst}/E_{disp} of the $L-ArBeO$, and the MEP of L . In any case, not unexpectedly, the *absolute* values of E_{disp} were totally uncorrelated with respect to the MEP.

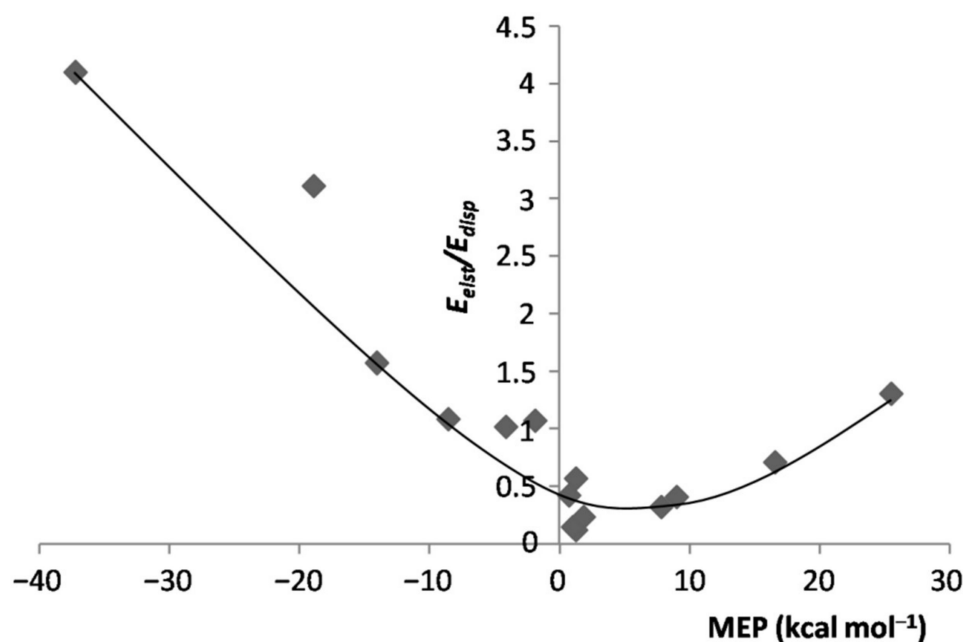


Figure 8. E_{elst}/E_{disp} ratio of the $L-ArBeO$ s vs. MEP at the $V_{S,max}/V_{S,min}$ of L .

4.4. Bonding Analysis of the LAr and the $L-ArBeO$

In keeping with the results of the SAPT analysis, all the presently-investigated LAr and $L-ArBeO$ were assigned as $nCov(C)$. Likewise, the exemplary N_2-Ar and linear $N_2-ArBeO$ shown in Figure 1, the $H^-(r)$ regions of any L and Ar or $ArBeO$, were, in fact, invariably well separated and plunged in a zone of positive values of $H(r)$; the latter was also invariably positive over Ω_s . However, as shown in Table 3, when going from any LAr to the corresponding $L-ArBeO$, the bond indices, particularly the $N(\Omega_s)$ and the $\rho_s(ave)$, underwent appreciable changes that were, in particular, clearly related to the changes occurring in their SAPT terms (vide supra). Thus, for the $Ng-ArBeO$ ($Ng = He, Ne, Ar$), the linear $N_2-ArBeO$, $OC-ArBeO$, $CO-ArBeO$, $ClF-ArBeO$, and $HF-ArBeO$, the T-shaped $F_2-ArBeO$ and $Cl_2-ArBeO$, and the C_{3v} isomer $H_3N-ArBeO$, the values of both $N(\Omega_s)$ and $\rho_s(ave)$ were higher than those predicted for the corresponding LAr . This suggests tighter interactions, well consistent with the SAPT prediction of $L-ArBeO$ complexes more stable than the LAr . On the other hand, for the T-shaped $N_2-ArBeO$, and the linear $F_2-ArBeO$ and $Cl_2-ArBeO$, the values of the two bond indices were lower than those predicted for the corresponding

*L*Ar, in good agreement with the lower stability of the *L*-ArBeO predicted by the SAPT analysis. This confirms the sensitivity of our proposed method in catching even subtle differences in the bonding character of the Ng complexes.

5. Conclusions

The comparison of the *L*-ArBeO with their “dispersive” cousins *L*Ar allowed us to highlight structural and stability effects peculiarly related to the σ -hole of ArBeO. Consistent with the electrostatic model of NCIs [16,59], the most-affected SAPT term was the E_{elst} . The values predicted for the *L*-ArBeO were clearly related to the values of the MEP at the $V_{S,max}$ or $V_{S,min}$ of *L*, and ranged from negative (attractive) to positive (repulsive) values depending on the negative/positive value of the MEP. The percentage contribution of E_{elst} may actually arrive up to ca 80% of the attractive interaction, and decisively determined the overall increased or decreased stability of any *L*-ArBeO with respect to the *L*Ar. The positive σ -hole of ArBeO also increased the inductive component of the interaction by an extent roughly related to the polarizability of *L*. The latter effects were, however, less pronounced than those occurring for the electrostatic component, the E_{ind} accounting for only ca. 9–21% of the overall stabilization. The nearly constant values of $E_{ind}(\%)$ actually resulted in a regular inverse dependence between the electrostatic and the dispersive component, even though the absolute contribution of E_{disp} was not directly correlated with the MEP of *L*. All these major effects become even clearer if one considers the bonding situation of the *L*Ar. In the absence of the σ -hole on Ar, the contribution of the electrostatic component was only minor, and nearly constant at around ca. 12–22% of the attractive stabilization. The interaction was, indeed, invariably dominated by the dispersion, even though the nearly null value of the electrostatic potential of Ar allowed us to recognize the direct influence of the MEP of *L* on the inductive component of the interaction. Our reached conclusions could be valid for other types of NCIs, especially those involving σ -holes of respectable strength such as those occurring in ArBeO. In this regard, there is, certainly, room for further future investigation.

Supplementary Materials: The following are available online. Table S1: MP2/aVTZ and CCSD(T)/aVTZAr-X distances and harmonic vibrational frequencies of the *L*Ar and *L*-ArBeO. Data S1: Cartesian coordinates of the *L*Ar and *L*-ArBeO. Table S2: MP2/aVTZ and CCSD(T)/aVTZ properties of the nCov(C) bonds of the *L*Ar and *L*-ArBeO. Table S3: Values of the MEP of *L* at the points of minimum ($V_{S,Min}$) or maximum ($V_{S,Max}$) calculated at the experimental, and at the CCSD(T)/aVTZ and MP2/aVTZ-optimized geometries. Figure S1: E_{ind} of the *L*Ar vs. MEP at the $V_{S,max}/V_{S,min}$ of *L*. Figure S2: $E_{ind}(\%)$ vs. $E_{disp}(\%)$ of the *L*Ar. Figure S3: $E_{disp}(\%)$ of the *L*Ar vs. MEP at the $V_{S,max}/V_{S,min}$ of *L*. Figure S4: $E_{elst}(\%)$ of the *L*-ArBeO vs. MEP at the $V_{S,max}/V_{S,min}$ of *L*. Figure S5: E_{ind} of the *L*-ArBeO vs. polarizability α of *L*. Figure S6: $E_{elst}(\%)$ vs. $E_{disp}(\%)$ of the *L*-ArBeO. Figure S7: $E_{disp}(\%)$ of the *L*-ArBeO vs. MEP at the $V_{S,max}/V_{S,min}$ of *L*.

Author Contributions: Methodology, data curation, software, S.B., F.G., N.S.; writing—original draft preparation, F.G.; writing—review and editing, S.B., N.S. All authors have read and agreed to the published version of the manuscript.

Funding: This research was funded by the Italian Ministry of Education, University and Research (MIUR) and the DIBAF Department of the University of Tuscia through the program “Departments of Excellence 2018–2022” (“Dipartimenti di Eccellenza 2018–2022”), grant “Landscape 4.0—food, wellbeing and environment”.

Institutional Review Board Statement: Not applicable.

Informed Consent Statement: Not applicable.

Data Availability Statement: Not applicable.

Conflicts of Interest: The authors declare no conflict of interest.

Sample Availability: Not available.

References

1. Hobza, P.; Müller-Dethlefs, K. *Noncovalent Interactions. Theory and Experiment*; RSC Theoretical and Computational Chemistry Series; Royal Society of Chemistry: Cambridge, UK, 2010.
2. *Noncovalent Interactions in the Synthesis and Design of New Compounds*; Maharramov, A.M.; Mahmudov, K.T.; Kopylovich, M.N.; Pombeiro, A.J.L. (Eds.) John Wiley and Sons: Hoboken, NJ, USA, 2016.
3. He, H.; Tan, W.; Guo, J.; Yi, M.; Shy, A.N.; Xu, B. Enzymatic Noncovalent Synthesis. *Chem. Rev.* **2020**, *120*, 9994–10078. [[CrossRef](#)]
4. Arunan, E.; Desiraju, G.R.; Klein, R.A.; Sadlej, J.; Scheiner, S.; Alkorta, I.; Clary, D.C.; Crabtree, R.H.; Dannenberg, J.J.; Hobza, P.; et al. Definition of the Hydrogen Bond (IUPAC Recommendations 2011). *Pure Appl. Chem.* **2011**, *83*, 1637–1641. [[CrossRef](#)]
5. Scheiner, S. Forty Years of Progress in the Study of the Hydrogen Bond. *Struct. Chem.* **2019**, *30*, 1119–1128. [[CrossRef](#)]
6. Clark, T.; Hennemann, M.; Murray, J.S.; Politzer, P. Halogen Bonding: The σ -Hole. *J. Mol. Model.* **2007**, *13*, 291–296. [[CrossRef](#)]
7. Clark, T. σ -Holes. *WIREs Comput. Mol. Sci.* **2013**, *3*, 13–20.
8. Politzer, P.; Murray, J.S.; Clark, T. Halogen Bonding and other σ -Hole Interactions: A Perspective. *Phys. Chem. ChemPhys.* **2013**, *15*, 11178–11189. [[CrossRef](#)]
9. Kolar, M.H.; Hobza, P. Computer Modeling of Halogen Bonds and other σ -Hole Interactions. *Chem. Rev.* **2016**, *116*, 5155–5187. [[CrossRef](#)]
10. Brammer, L. Halogen Bonding, Chalcogen Bonding, Pnictogen Bonding, Tetrel Bonding: Origins, Current Status and Discussion. *Faraday Discuss.* **2017**, *203*, 485–507. [[CrossRef](#)]
11. Dong, W.; Li, Q.; Scheiner, S. Comparative Strengths of Tetrel, Pnictogen, Chalcogen, and Halogen Bonds and Contributing Factors. *Molecules* **2018**, *23*, 1681. [[CrossRef](#)]
12. Desiraju, G.R.; Ho, P.S.; Kloo, L.; Legon, A.C.; Marquardt, R.; Metrangolo, P.; Politzer, P.; Resnati, G.; Rissanen, K. Definition of the Halogen Bond (IUPAC Recommendations 2013). *Pure Appl. Chem.* **2013**, *85*, 1711–1713. [[CrossRef](#)]
13. Cavallo, G.; Metrangolo, P.; Milani, R.; Pilati, T.; Priimagi, A.; Resnati, G.; Terraneo, G. The Halogen Bond. *Chem. Rev.* **2016**, *116*, 2478–2601. [[CrossRef](#)]
14. Parajuli, R. Does the Recent IUPAC Definition of Hydrogen Bonding Lead to New Intermolecular Interactions? *Curr. Sci.* **2016**, *110*, 495–498.
15. Alkorta, I.; Elguero, J.; Frontera, A. Not only Hydrogen Bonds: Other Noncovalent Interactions. *Crystals* **2020**, *10*, 180. [[CrossRef](#)]
16. Murray, J.S.; Politzer, P. Molecular Electrostatic Potentials and Noncovalent Interactions. *WIREs Comput. Mol. Sci.* **2017**, *7*, e1326. [[CrossRef](#)]
17. Bader, R.F.; Carroll, M.T.; Cheeseman, J.R.; Chang, C. Properties of Atoms in Molecules: Atomic Volumes. *J. Am. Chem. Soc.* **1987**, *109*, 7968–7979. [[CrossRef](#)]
18. Borocci, S.; Grandinetti, F.; Sanna, N. From LAr to L-ArBeO (L = He, Ne, Ar, HF): Switching on σ -Hole Effects in Non-Covalent Interactions. *Chem. Phys. Lett.* **2021**, *768*, 138402. [[CrossRef](#)]
19. Grandinetti, F. *Noble Gas. Chemistry: Structure, Bonding, and Gas-Phase Chemistry*; Wiley-VCH: Weinheim, Germany, 2018; Chapter 3; pp. 100–107.
20. Jeziorski, B.; Moszyński, R.; Ratkiewicz, A.; Rybak, V.; Szalewicz, K.; Williams, H.L. *Methods and Techniques in Computational Chemistry: METECC-94*; Clementi, E., Ed.; STEF: Cagliari, Italy, 1993; Volume B.
21. Jeziorski, B.; Moszyński, R.; Szalewicz, K. Perturbation Theory Approach to Intermolecular Potential Energy Surfaces of van der Waals Complexes. *Chem. Rev.* **1994**, *94*, 1887–1930. [[CrossRef](#)]
22. Borocci, S.; Giordani, M.; Grandinetti, F. Bonding Motifs of Noble-Gas Compounds as Described by the Local Electron Energy Density. *J. Phys. Chem. A* **2015**, *119*, 6528–6541. [[CrossRef](#)] [[PubMed](#)]
23. Borocci, S.; Grandinetti, F.; Sanna, N.; Antoniotti, P.; Nunzi, F. Non-Covalent Complexes of the Noble-Gas Atoms: Analyzing the Transition from Physical to Chemical Interactions. *J. Comput. Chem.* **2019**, *40*, 2318–2328. [[CrossRef](#)]
24. Borocci, S.; Grandinetti, F.; Sanna, N.; Nunzi, F. Classifying the Chemical Bonds Involving the Noble-Gas Atoms. *New J. Chem.* **2020**, *44*, 14536–14550. [[CrossRef](#)]
25. Murray, J.S.; Shields, Z.P.I.; Seybold, P.G.; Politzer, P. Intuitive and Counterintuitive Noncovalent Interactions of Aromatic π Regions with the Hydrogen and the Nitrogen of HCN. *J. Comput. Sci.* **2015**, *10*, 209–216. [[CrossRef](#)]
26. Wang, C.; Danovich, D.; Shaik, S.; Wu, W.; Mo, Y. Attraction between Electrophilic Caps: A Counterintuitive Case of Noncovalent Interactions. *J. Comput. Chem.* **2019**, *40*, 1015–1022. [[CrossRef](#)]
27. Cremer, D.; Kraka, E. Chemical Bonds without Bonding Electron Density—Does the Difference Electron-Density Analysis Suffice for a Description of the Chemical Bond? *Angew. Chem. Int. Ed. Engl.* **1984**, *23*, 627–628. [[CrossRef](#)]
28. Cremer, D.; Kraka, E. A Description of the Chemical Bond in Terms of Local Properties of Electron Density and Energy. *Croat. Chem. Acta* **1984**, *57*, 1259–1281.
29. Johnson, E.R.; Keinan, S.; Mori-Sanchez, P.; Contreras-Garcia, J.; Cohen, A.J.; Yang, W. Revealing Noncovalent Interactions. *J. Am. Chem. Soc.* **2010**, *132*, 6498–6506. [[CrossRef](#)] [[PubMed](#)]
30. Narth, C.; Maroun, Z.; Boto, R.A.; Chaudret, R.; Bonnet, M.L.; Piquemal, J.-P.; Contreras-García, J. A Complete NCI Perspective: From New Bonds to Reactivity. In *Applications of Topological Methods in Molecular Chemistry*; Springer: Cham, Switzerland, 2016; pp. 491–527.
31. Bader, R.F.W. *Atoms in Molecules: A Quantum Theory*; Oxford University Press: Oxford, UK, 1990.

32. Borocci, S.; Grandinetti, F.; Sanna, N.; Antoniotti, P.; Nunzi, F. Complexes of Helium with Neutral Molecules: Progress toward a Quantitative Scale of Bonding Character. *J. Comput. Chem.* **2020**, *41*, 1000–1011. [CrossRef]
33. Møller, C.; Plesset, M.S. Note on an Approximation Treatment for Many-Electron Systems. *Phys. Rev.* **1934**, *46*, 618. [CrossRef]
34. Raghavachari, K.; Trucks, G.W.; Pople, J.A.; Head-Gordon, M. A Fifth-Order Perturbation Comparison of Electron Correlation Theories. *Chem. Phys. Lett.* **1989**, *157*, 479–483. [CrossRef]
35. Pritchard, B.P.; Altarawy, D.; Didier, B.; Gibson, T.D.; Windus, T.L. New Basis Set Exchange: An Open, Up-To-Date Resource for the Molecular Sciences Community. *J. Chem. Inf. Model.* **2019**, *59*, 4814–4820. [CrossRef] [PubMed]
36. Frisch, M.J.; Trucks, G.W.; Schlegel, H.B.; Scuseria, G.E.; Robb, M.A.; Cheeseman, J.R.; Scalmani, G.; Barone, V.; Mennucci, B.; Petersson, G.A.; et al. *Gaussian 09, Revision D.01*; Gaussian Inc.: Wallingford, CT, USA, 2013.
37. Welcome to the Website of CFOUR. Available online: <http://www.cfour.de> (accessed on 20 July 2021).
38. Bukowski, R.; Cencek, W.; Jankowski, P.; Jeziorska, M.; Jeziorski, B.; Kucharski, S.A.; Lotrich, V.F.; Metz, M.P.; Misquitta, A.J.; Moszyński, R.; et al. *SAPT2016: An Ab Initio Program for Symmetry-Adapted Perturbation Theory Calculations of Intermolecular Interactions Energies. Sequential and Parallel Versions*; University of Delaware: Newark, DE, USA; University of Warsaw: Warsaw, Poland, 2016.
39. Tao, F.-M.; Pan, Y.-K. Ab Initio Potential Energy Curves and Binding Energies of Ar₂ and Mg₂. *Mol. Phys.* **1994**, *81*, 507–518. [CrossRef]
40. Tao, F.-M.; Klemperer, W. Accurate ab Initio Potential Energy Surfaces of Ar–HF, Ar–H₂O, and Ar–NH₃. *J. Chem. Phys.* **1994**, *101*, 1129–1145. [CrossRef]
41. Saleh, G.; Gatti, C.; Lo Presti, L. Energetics of Non-Covalent Interactions from Electron and Energy Density Distributions. *Comput. Theor. Chem.* **2015**, *1053*, 53–59. [CrossRef]
42. Lu, T.; Chen, F. Multiwfn: A Multifunctional Wavefunction Analyzer. *J. Comput. Chem.* **2012**, *33*, 580–592. [CrossRef] [PubMed]
43. Zou, W. Molden2AIM. Available online: <https://github.com/zorkzou/Molden2AIM> (accessed on 01 February 2021).
44. Lee, T.J.; Taylor, P.R. A Diagnostic for Determining the Quality of Single-Reference Electron Correlation Methods. *Int. J. Quantum Chem.* **1989**, *36*, 199–207. [CrossRef]
45. Keil, M.; Danielson, L.J.; Dunlop, P.J. On Obtaining Interatomic Potentials from Multiproperty Fits to Experimental Data. *J. Chem. Phys.* **1991**, *94*, 296–309. [CrossRef]
46. Barrow, D.A.; Aziz, R.A. The Neon-Argon Potential Revisited. *J. Chem. Phys.* **1988**, *89*, 6189–6194. [CrossRef]
47. Aziz, R.A. A Highly Accurate Interatomic Potential for Argon. *J. Chem. Phys.* **1993**, *99*, 4518–4525. [CrossRef]
48. Dham, A.K.; Meath, W.J.; Jechow, J.W.; McCourt, F.R.W. New Exchange-Coulomb N₂-Ar Potential-Energy Surface and its Comparison with other Recent N₂-Ar Potential-Energy Surfaces. *J. Chem. Phys.* **2006**, *124*, 034308. [CrossRef]
49. Sumiyoshi, Y.; Endo, Y. Three-Dimensional Potential Energy Surface of Ar-CO. *J. Chem. Phys.* **2015**, *142*, 024314. [CrossRef]
50. Chan, K.W.; Power, T.D.; Jai-nhuknan, J.; Cybulski, S.M. An *ab Initio* Study of He-F₂, Ne-F₂, and Ar-F₂ van der Waals Complexes. *J. Chem. Phys.* **1999**, *110*, 860–869. [CrossRef]
51. Rohrbacher, A.; Janda, K.C.; Beneventi, L.; Casavecchia, P.; Volpi, G.G. Differential Scattering Cross Sections for HeCl₂, NeCl₂, and ArCl₂: Multiproperty Fits of Potential Energy Surfaces. *J. Phys. Chem. A* **1997**, *101*, 6528–6537. [CrossRef]
52. Prosmi, R.; Villareal, P.; Delgado-Barrio, G. Structure and Bonding of ArClF: Intermolecular Potential Surface. *Isr. J. Chem.* **2003**, *43*, 279–286. [CrossRef]
53. Hutson, J.M. Vibrational Dependence of the Anisotropic Intermolecular Potential of Ar-HF. *J. Chem. Phys.* **1992**, *96*, 6752–6767. [CrossRef]
54. Jouypazadeh, H.; Solimannejad, M.; Farrokhpour, H. New Potential Energy Surface and Rovibrational Spectra of Ar⋯HCl. *Comput. Theor. Chem.* **2016**, *1083*, 64–71. [CrossRef]
55. Loreau, J.; Liévin, J.; Scribano, Y.; van der Avoird, A. Potential Energy Surface and Bound States of the NH₃-Ar and ND₃-Ar Complexes. *J. Chem. Phys.* **2014**, *141*, 224303. [CrossRef]
56. Chałasiński, G.; Szczyński, M.M. Origins of Structure and Energetics of van der Waals Clusters from *ab Initio* Calculations. *Chem. Rev.* **1994**, *94*, 1723–1765. [CrossRef]
57. Nunzi, F.; Pannacci, G.; Tarantelli, F.; Belpassi, L.; Cappelletti, D.; Falcinelli, S.; Pirani, F. Leading Interaction Components in the Structure and Reactivity of Noble Gases Compounds. *Molecules* **2020**, *25*, 2367. [CrossRef] [PubMed]
58. Maroulis, G. Accurate Electric Multipole Moment, Static Polarizability and Hyperpolarizability Derivatives for N₂. *J. Chem. Phys.* **2003**, *118*, 2673–2687. [CrossRef]
59. Maroulis, G. Electric Polarizability and Hyperpolarizability of Carbon Monoxide. *J. Phys. Chem.* **1996**, *100*, 13466–13473. [CrossRef]
60. Maroulis, G. On the Bond-Length Dependence of the Static Electric Polarizability and Hyperpolarizability of F₂. *Chem. Phys. Lett.* **2007**, *442*, 265–269. [CrossRef]
61. Maroulis, G. Accurate Dipole Polarizability for Cl₂ (X¹Σ_g⁺). *Mol. Phys.* **1992**, *77*, 1085–1094. [CrossRef]
62. Miller, K.J.; Savchik, J.A. A New Empirical Method to Calculate Average Molecular Polarizabilities. *J. Am. Chem. Soc.* **1979**, *101*, 7206–7213. [CrossRef]
63. Sadlej, A.J. Electric Properties of Diatomic Interhalogens. A Study of the Electron Correlation and Relativistic Contributions. *J. Chem. Phys.* **1992**, *96*, 2048–2053. [CrossRef]

64. Maroulis, G. Electric Multipole Moment, Dipole and Quadrupole (Hyper)Polarizability Derivatives for HF ($X^1\Sigma^+$). *J. Mol. Struct. (THEOCHEM)* **2003**, *633*, 177–197. [[CrossRef](#)]
65. Maroulis, G. A Systematic Study of Basis Set, Electron Correlation, and Geometry Effects on the Electric Multipole Moments, Polarizability, and Hyperpolarizability of HCl. *J. Chem. Phys.* **1998**, *108*, 5432–5448. [[CrossRef](#)]
66. Zeiss, G.D.; Meath, W.J. Dispersion Energy Constants C_6 (A,B), Dipole Oscillator Strength Sums and Refractivities for Li, N, O, H₂, N₂, O₂, NH₃, H₂O, NO and N₂O. *Mol. Phys.* **1977**, *33*, 1155–1176. [[CrossRef](#)]
67. Clark, T. Polarization, Donor-Acceptor Interactions, and Covalent Contributions in Weak Interactions: A Clarification. *J. Mol. Model.* **2017**, *23*, 297. [[CrossRef](#)] [[PubMed](#)]
68. Murray, J.S.; Politzer, P. Interaction and Polarization Energy Relationships in σ -Hole and π -Hole Bonding. *Crystals* **2020**, *10*, 76. [[CrossRef](#)]